High Power Laser Science and Engineering, (2025), Vol. 13, e59, 15 pages.
doi:10.1017/hpl.2025.10037

HIGH POWER LASER SCIENCE AND ENGINEERING

RESEARCH ARTICLE

Spatial distributions of laser–plasma instability in the beam overlapping region

Chengzhuo Xiao[1,3], Kaiqiang Pan[2], Han Wen[1], Tao Gong[2], Zhichao Li[2], Ji Yan[2], Jinqing Yu[1], and Dong Yang[2]

[1]*School of Physics and Electronics, Hunan University, Changsha, China*

[2]*National Key Laboratory of Plasma Physics, Laser Fusion Research Center, China Academy of Engineering Physics, Mianyang, China*

[3]*Collaborative Innovation Center of IFSA (CICIFSA), Shanghai Jiao Tong University, Shanghai, China*

(Received 25 November 2024; revised 1 May 2025; accepted 15 May 2025)

Abstract

A reduced dispersion relation for multibeam laser–plasma instability is derived. The dispersion relation includes the combined effects of self-coupling and interaction with other beams by sharing a common scattered light (SL modes) and by sharing a common plasma wave (SP modes). The latter two have the most prominent collective effects of all. We have solved the dispersion relation numerically for stimulated Raman scattering, and set different beam configurations and polarizations to discuss the spatial distributions of the temporal growth rate. The instability in the beam overlapping region is complicated, but there are still a few simple rules that govern the system, such as the dominancy of SL modes and subdominancy of backscattering and SP modes. The maximum growth rate always occurs at these special modes, or a new mode formed by combining two or three of the special modes. The reduced model provides us with the ability to understand the underlying physics of multibeam instabilities under general laser and plasma conditions.

Keywords: inertial confinement fusion; multiple laser beams; stimulated Brillouin scattering; stimulated Raman scattering

1. Introduction

Laser propagating in under-dense plasma may trigger instabilities such as stimulated Raman scattering (SRS) and stimulated Brillouin scattering (SBS) where the laser decays into a scattered light and a plasma wave[1]. The laser–plasma instability (LPI) is one of the most troublesome obstacles to inertial confinement fusion (ICF). To achieve fusion, hundreds of laser beams are required to symmetrically irradiate the target, and these beams would inevitably overlap in plasma, forming a unique beam overlapping region different from the single-beam propagating region. The instability there is what we called the multibeam LPI[2].

Multibeam LPIs include many existing instabilities, such as cross-beam energy transfer (CBET)[3–5], which is two-beam SBS, and multibeam two-plasmon decay (TPD)[6–10], which is also based on two-beam interaction. More beams may introduce brand new features, such as unexpected scattering geometries[11–13], strengthened and collimating electron plasma waves[14–16]. There are two special modes associated with multibeam effects, one with a shared scattered light, which is called the SL mode, and the other with a shared plasma wave, which is called the SP mode[17]. The two modes constitute most of the dominant modes in the beam overlapping region. The multibeam instability strongly relies on the beam number, configurations and polarizations, so understanding the instability growth in the beam overlapping region with a general condition is of great importance, but it is still an open question. The dominant mode could be the SL mode, SP mode, backscattering, or another multibeam mode. A general method to determine the growth rates of all these modes is the key point to solve the problem.

Recently, we derived a general dispersion relation for multibeam SRS and SBS with an arbitrary beam number, configurations and polarizations, and obtained analytic

Correspondence to: C. Xiao, School of Physics and Electronics, Hunan University, Changsha 410082, China. Email: xiaocz@hnu.edu.cn; T. Gong, National Key Laboratory of Plasma Physics, Laser Fusion Research Center, China Academy of Engineering Physics, Mianyang 621900, China. Email: gongtaolfrc@163.com

growth rates for some special cases[18]. Although the general dispersion relation in the form of a determinant is largely simplified from the full dispersion relation of the (N^2-N+1)th-order matrix to the Nth-order matrix, numerical calculation is still unrealistic for large beam numbers $N>2$. In this paper, the determinant of the Nth-order matrix is further simplified to the summation over all beams, reducing the basic calculations from $(N^2-N+1)!$ to $N!$ and finally to a maximum of $N(2N-1)$, which is easier for numerical calculations. The dispersion relation includes three main interactions, the self-coupling term, SL mode terms and SP mode terms, so we use it to study the spatial distributions of the SRS growth rate under various beam configurations and polarizations.

The 100 kJ laser facility in China[19] is used here, where four cones of 28.5°, 35°, 49.5° and 55° of a total of 48 beams are arbitrarily chosen either with s-polarization or p-polarization. A study with two-, four- and eight-beam interactions shows the complexity of multibeam instability growth. We have also discussed a backward seed with the same polarization with its incident beam propagating through the beam overlapping region. The backward scattering is compared with the multibeam modes. From the results, we can deduce some simple features for multibeam instability. Firstly, backward scattering is usually not the dominant mode in the beam overlapping region, especially when the number of beams is larger than two. Secondly, in most cases SL modes dominate the beam overlapping region. Particularly for the symmetric case, the shared scattered light coming from the polar axis (symmetric axis) has the maximum growth rate. Thirdly, SP modes could dominate the system when the coupling is less efficient and the incidence angle is small. Last but not least, there are some other collective modes resulting from the combination of two or three special modes that would scatter from other directions. These modes exist when the coupling is not very efficient. The rules provide us with a simple method to estimate the instability growth in the beam overlapping region. Particle-in-cell (PIC) simulations are also performed to verify the spatial distribution obtained by the reduced model. It shows that our reduced model is in good agreement with two-dimensional (2D) PIC simulations, and has the advantage of simulating more beams in three dimensions with less simulation time.

The paper is organized as follows. In Section 2, a reduced dispersion relation is derived. The key point of the polarization factor in the dispersion relation is established before we numerically solve the dispersion relation. In Section 3 we discuss the distribution of the SRS growth rate under various conditions, in order to understand the physics of multibeam instability step-by-step. Then we summarize and induce some simple rules valid for most common multibeam situations in Section 4. To verify the reduced model, 2D PIC simulations are also performed in Section 5. Finally, conclusions are given in Section 6.

2. Reduced dispersion relation for multibeam laser–plasma instability

The dispersion relation for SRS or SBS in multiple laser beams with arbitrary beam numbers, polarizations and configurations has been derived recently, in the form of a determinant[18], as follows:

$$\begin{vmatrix} \frac{1}{\mu^{11}_{k-\Delta K_{i_0 1}}} & -1 & \cdots & -1 \\ -1 & \frac{1}{\mu^{22}_{k-\Delta K_{i_0 2}}} & \cdots & -1 \\ \vdots & \vdots & & \vdots \\ -1 & -1 & \cdots & \frac{1}{\mu^{NN}_{k-\Delta K_{i_0 N}}} \end{vmatrix} = 0, \tag{1}$$

where the diagonal elements of the coefficient matrix are given by the following:

$$\frac{1}{\mu^{j_0 j_0}_{k-\Delta K_{i_0 j_0}}} = \frac{D_{\mathrm{p}}\left(\vec{k}-\Delta\vec{K}_{i_0 j_0},\omega\right) - \left|\vec{k}-\Delta\vec{K}_{i_0 j_0}\right|^2 \Gamma_0^2 \sum_{i=1}^{N} \frac{\cos^2\phi_{0i}}{D_{\mathrm{l}}\left(\vec{k}-\Delta\vec{K}_{i_0 j_0}-\vec{K}_{0i},\omega-\omega_0\right)}}{\left|\vec{k}-\Delta\vec{K}_{i_0 j_0}\right|^2 \Gamma_0^2 \frac{\cos^2\phi_{0 j_0}}{D_{\mathrm{l}}\left(\vec{k}-\vec{K}_{0 i_0},\omega-\omega_0\right)}}. \tag{2}$$

It is reduced from the full dispersion relation in a form of a determinant of the (N^2-N+1)th-order matrix, but still intractable when the beam number N is large. It describes the interactions of a particular beam i_0 with all N beams, including the coupling with itself. The incident laser beams have the same frequency ω_0 but different wave vectors $\vec{K}_{0i}$, and the vector difference is $\Delta\vec{K}_{i_0 j_0}=\vec{K}_{0 i_0}-\vec{K}_{0 j_0}$. The coupling coefficients Γ_0 could represent either SRS, $\Gamma_0^2=v_0^2\omega_{\mathrm{pe}}^2/4$, or SBS, $\Gamma_0^2=v_0^2\omega_{\mathrm{pi}}^2/4$, respectively, where v_0 is the quiver velocity of the electron in a laser and ω_{pe}, ω_{pi} are the electron and ion plasma frequency, respectively. The kernels are dispersion functions representing the properties of decay waves. Here, D_{l} represents the light wave dispersion function, $D_{\mathrm{l}}(\vec{k},\omega)=-\omega^2-2i\nu_{\mathrm{s}}\omega+c^2k^2+\omega_{\mathrm{pe}}^2$, D_{p} represents the plasma wave, either a Langmuir wave, $D_{\mathrm{p}}(\vec{k},\omega)=-\omega^2-2i\nu_{\mathrm{e}}\omega+3v_{\mathrm{e}}^2k^2+\omega_{\mathrm{pe}}^2$, or an ion acoustic wave, $D_{\mathrm{p}}(\vec{k},\omega)=-\omega^2-2i\nu_{\mathrm{i}}\omega+c_{\mathrm{s}}^2k^2$, ν is the phenomenological damping rate and $c, v_{\mathrm{e}}, c_{\mathrm{s}}$ are light speed, electron thermal velocity and ion sound velocity, respectively. The trickiest term discussed in this paper is $\cos\phi_{0i}$, the polarization factor, which will be defined and explained later.

In Ref. [18] we derived analytic results of the dispersion relation for two special cases, one with a shared scattered light, also called the SL mode, and the other with a shared

https://doi.org/10.1017/hpl.2025.10037 Published online by Cambridge University Press

plasma wave, called the SP mode. Other than these two special modes, the analytic growth rate of any scattering geometry is unavailable. Therefore, numerical calculations of Equation (1) are desperately needed to obtain the whole distribution of the growth rate in three dimensions. To make it feasible for numerical calculation, we further reduce the dispersion relation to a simpler form. Equation (1) can be transformed into the following:

$$1=\sum_{j_0=1}^{N}\frac{1}{\varepsilon_{j_0}}, \tag{3}$$

after some algebra, where $\varepsilon_{j_0}=1+1/\mu^{j_0j_0}_{k-\Delta K_{i_0j_0}}$. Equation (3) is equivalent to Equation (1) but in a more simplified form; however, we note that there is a double summation on the denominator, which is difficult for calculation. Therefore, we should further reduce the dispersion relation using its resonant properties. The inner summation is over the variable i in the formula of $1/\mu^{j_0j_0}_{k-\Delta K_{i_0j_0}}$, while the outer summation is over j_0. When $j_0\neq i_0$, we only consider the term $i=j_0$ in the inner summation, since it is non-resonant for $i\neq j_0$ and $j_0\neq i_0$. When $j_0=i_0$, the inner summation should be fully considered. After the approximation, Equation (3) is rewritten as follows:

$$1=\sum_{j_0=1,j_0\neq i_0}^{N}\frac{\left|\vec{k}-\Delta\vec{K}_{i_0j_0}\right|^2\Gamma_0^2\cos^2\phi_{0j_0}}{D_{\rm p}\left(\vec{k}-\Delta\vec{K}_{i_0j_0},\omega\right)D_{\rm l}\left(\vec{k}-\vec{K}_{0i_0},\omega-\omega_0\right)} +\frac{k^2\Gamma_0^2\dfrac{\cos^2\phi_{0i_0}}{D_{\rm p}\left(\vec{k},\omega\right)D_{\rm l}\left(\vec{k}-\vec{K}_{0i_0},\omega-\omega_0\right)}}{1-k^2\Gamma_0^2\sum_{i=1,i\neq i_0}^{N}\dfrac{\cos^2\phi_{0i}}{D_{\rm p}\left(\vec{k},\omega\right)D_{\rm l}\left(\vec{k}-\vec{K}_{0i},\omega-\omega_0\right)}}. \tag{4}$$

The double summation is now reduced to the single summation; however, one of the summations is still on the denominator. We could further turn this term into numerator by multiplying it on each side and noting that the terms in $\sum\times\sum$ are negligible compared with other terms, which are all zero or first order. Finally, we get to a simpler and more physical dispersion relation for multibeam LPI:

$$\begin{aligned}1=&k^2\Gamma_0^2\frac{\cos^2\phi_{0i_0}}{D_{\rm p}\left(\vec{k},\omega\right)D_{\rm l}\left(\vec{k}-\vec{K}_{0i_0},\omega-\omega_0\right)}\\&+\sum_{j_0=1,j_0\neq i_0}^{N}\frac{\left|\vec{k}-\Delta\vec{K}_{i_0j_0}\right|^2\Gamma_0^2\cos^2\phi_{0j_0}}{D_{\rm p}\left(\vec{k}-\Delta\vec{K}_{i_0j_0},\omega\right)D_{\rm l}\left(\vec{k}-\vec{K}_{0i_0},\omega-\omega_0\right)}\\&+k^2\Gamma_0^2\sum_{i=1,i\neq i_0}^{N}\frac{\cos^2\phi_{0i}}{D_{\rm p}\left(\vec{k},\omega\right)D_{\rm l}\left(\vec{k}-\vec{K}_{0i},\omega-\omega_0\right)}.\end{aligned} \tag{5}$$

The physics of the dispersion relation is clearly demonstrated: the first term on the right-hand side (RHS) is the self-matching or single-beam term of beam i_0; the second term on the RHS represents the interaction of other beams with beam i_0 while sharing a common scattered light, $D_{\rm l}(\vec{k}-\vec{K}_{0i_0},\omega-\omega_0)$; the third term is the counterpart of the second term but sharing a common plasma wave, $D_{\rm p}(\vec{k},\omega)$. Therefore, the reduced dispersion relation considers the leading parts of the beam interactions, which includes contributions of the single-beam and shared decay waves, and only has a calculation of $2N-1$, which is much easier for numerical calculation. The dispersion relation could also be transformed to a reference frame of scattered light, where $\vec{k}$ and ω are solved for the scattered light. The detailed derivation of such dispersion relation is presented in the Appendix.

One should also note that the reduced dispersion relation is for a particular beam i_0 due to the simplification of the full (N^2-N+1)th-order matrix to an Nth-order matrix[18]. Solving the reduced dispersion relation for beam i_0, we can obtain the growth rates describing properties of the multibeam system; however, it will lose some special modes excited by other beams. Therefore, to get a complete picture of the multibeam system, the calculation over all beams (i.e., a loop from $i_0=1$ to N) is needed, especially when beams are different.

2.1. *Some special solutions*

The dispersion relation is analytic solvable under the following cases. Firstly, for single-beam interaction, $N=1$, the dispersion relation is given by the following:

$$1=k^2\Gamma_0^2\frac{\cos^2\phi_{0i_0}}{D_{\rm p}\left(\vec{k},\omega\right)D_{\rm l}\left(\vec{k}-\vec{K}_{0i_0},\omega-\omega_0\right)}. \tag{6}$$

Let us assume $\omega=\omega_k+i\gamma$, where ω_k is the frequency of the plasma wave with wave number k and γ is the growth rate. For weak coupling $\gamma\ll\omega_k$ and neglecting damping, the dispersion functions are approximated by $D_{\rm p}\approx-2i\gamma\omega_k$ and $D_{\rm l}\approx 2i\gamma(\omega_0-\omega_k)$. It is now possible to get the single-beam growth rate, $\gamma_0=\frac{kv_0}{4}\sqrt{\frac{\omega^2_{{\rm pe},i}}{\omega_k(\omega_0-\omega_k)}}$, where the polarization factor could be unity.

For $N>1$, there are two special cases with analytic results. If the first and second terms of Equation (5) could be resonant, while the third term is non-resonant, we neglect the non-resonant term and obtain the following:

$$1=\sum_{j_0=1}^{N}\frac{\left|\vec{k}-\Delta\vec{K}_{i_0j_0}\right|^2\Gamma_0^2\cos^2\phi_{0j_0}}{D_{\rm p}\left(\vec{k}-\Delta\vec{K}_{i_0j_0},\omega\right)D_{\rm l}\left(\vec{k}-\vec{K}_{0i_0},\omega-\omega_0\right)}. \tag{7}$$

https://doi.org/10.1017/hpl.2025.10037 Published online by Cambridge University Press

An analytic result emerges when $|\vec{k} - \Delta\vec{K}_{i_0j_0}| = |k|$ for $j_0 = 1,\ldots,N$, so both D_l and D_p could be resonant at the same time. We have $D_\mathrm{l}(\vec{k} - \vec{K}_{0i_0}, \omega - \omega_0) \approx 2i\gamma(\omega_0 - \omega_k)$ and $D_\mathrm{p}(\vec{k} - \Delta\vec{K}_{i_0j_0}, \omega) = D_\mathrm{p}(k,\omega) \approx -2i\gamma\omega_k$. The multibeam growth rate is then given by the following:

$$\gamma_{\mathrm{SL}}^2 = \frac{k_{\mathrm{SL}}^2\Gamma_0^2}{4\omega_k(\omega_0 - \omega_k)}\sum_{j_0=1}^{N}\cos^2\phi_{0j_0}. \tag{8}$$

The wave number k_{SL} satisfies the condition $|\vec{k} - \Delta\vec{K}_{i_0j_0}| = |k|$ for $j_0 = 1,\ldots,N$, which indicates that all beams share a common scattered light[18]. This is the so-called SL mode.

On the other hand, when resonance occurs in the first and the third terms of Equation (5), the dispersion relation becomes the following:

$$1 = k^2\Gamma_0^2\sum_{i=1}^{N}\frac{\cos^2\phi_{0i}}{D_\mathrm{p}\left(\vec{k},\omega\right)D_\mathrm{l}\left(\vec{k} - \vec{K}_{0i}, \omega - \omega_0\right)}. \tag{9}$$

Similarly, if $|\vec{k} - \vec{K}_{0i}| = |\vec{k} - \vec{K}_{0j}|$ for any two beams, D_l and D_p could also be resonant with $D_\mathrm{l} \approx 2i\gamma(\omega_0 - \omega_k)$ and $D_\mathrm{p} \approx -2i\gamma\omega_k$, and the growth rate is given by the following:

$$\gamma_{\mathrm{SP}}^2 = \frac{k_{\mathrm{SP}}^2\Gamma_0^2}{4\omega_k(\omega_0 - \omega_k)}\sum_{i=1}^{N}\cos^2\phi_{0i}, \tag{10}$$

where k_{SP} satisfies the condition $|\vec{k} - \vec{K}_{0i}| = |\vec{k} - \vec{K}_{0j}|$ for any i and j, which implies all beams can share a common plasma wave[18], or the so-called SP mode. The growth rates of the SL mode in Equation (8) and SP mode in Equation (10) have the same form, but are different in terms of the wave number of the plasma wave and the polarization factor.

2.2. *Roles of polarization*

The multibeam dispersion relation relies heavily on the polarizations of incident beams, and the polarization of the scattered light is a degree of freedom, so we should deal with the polarization carefully. In the reduced dispersion relation, the polarization effect is imbedded in the factor $\cos\phi_{0i} = \hat{e}_{0i}\cdot\hat{e}_\mathrm{s}$, where $\hat{e}_{0i}$ denotes the unit vector of the polarization direction of beam i and $\hat{e}_\mathrm{s}$ is the unit vector of the polarization direction of the corresponding scattered light. Here the scattered light should be coincident with its light wave dispersion function, that is, the one on its denominator.

Here, $\hat{e}_\mathrm{s}$ is an undetermined variable for each scattered light, which needs to be determined first before calculating the growth rate. There are two possible ways to do that. (1) Assuming the seed scattered light has all kinds of polarization directions perpendicular to its propagation direction, the one that brings the highest growth rate wins the game. We call it the maximum-growth-rate principle (MGRP). (2) The seed with a specific polarization direction passes through the overlapping region, growing with a growth rate determined by the multibeam dispersion relation. This special seed could be backscattered light growing from the single-beam region, the seed electromagnetic waves from Thomson scattering[20], etc.

We consider both cases in our calculations. For the single-beam LPI, $N = 1$, the MGRP immediately shows that $\cos^2\phi_{0i_0} = 1$ in Equation (6). Therefore, the scattered light (mostly backscatter) has the same polarization direction as the incident light. The backscattering of beam i_0 propagates in the beam overlapping region, and we compare its growth rate with the multibeam modes later. For multibeam LPI, the reduced dispersion relation, Equation (5), becomes much more complicated. We should determine the polarization directions of N scattered lights by using the MGRP, and note that the polarization direction of each scattered light becomes a degree of freedom. It is difficult to do this numerically, so instead we use reasonable approximations to obtain the polarization directions of N scattered lights. For the common scattered light $D_\mathrm{l}(\vec{k} - \vec{K}_{0i_0}, \omega - \omega_0)$, we search for its polarization direction by finding the maximum of $\sum_{j_0=1}^{N}\cos^2\phi_{0j_0}$ according to Equation (8). Meanwhile, for the other $N-1$ scattered lights, each scattered light could search for its maximum coupling with its own incident beam, individually, that is, finding the maximum of $\cos^2\phi_{0i}$ to determine the polarization direction of each scattered light, $D_\mathrm{l}(\vec{k} - \vec{K}_{0i}, \omega - \omega_0)$, $i = 1,2,\ldots,N$, $i \neq i_0$.

Discussing how polarizations of multiple beams affect the distribution of temporal growth rate in three dimensions is one of our main goals of this paper. By numerically solving the reduced model with the above polarization determining schemes, we will see that in the next section.

3. Numerical results for multibeam growth rates

3.1. *Numerical settings and benchmark via single-beam instability*

In this section, distributions of the SRS temporal growth rates for one, two, four and eight beams under a variety of polarization combinations are numerically calculated and discussed. Our intention is to understand the underlying physics of the instability growth in the ambience of multiple overlapping laser beams, and obtain general laws characterizing the distributions and maximums of the growth rate under different polarizations.

Equation (5) is numerically solved for SRS in homogeneous plasmas. The spatial distribution is not sensitive to the plasma conditions and laser intensity, so we choose

https://doi.org/10.1017/hpl.2025.10037 Published online by Cambridge University Press

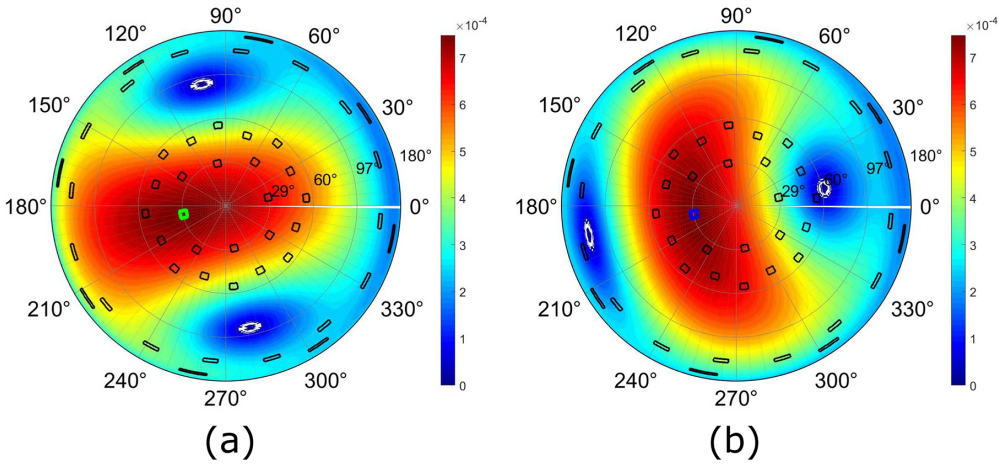

Figure 1. Spatial distributions of the single-beam SRS growth rate: (a) s-polarized beam denoted by the green rectangle and (b) p-polarized beam denoted by the blue rectangle. The unit of the growth rate is ω_0^{-1}.

typical parameters in ICF, $n_e = 0.1n_c$, $T_e = 2\text{keV}$ and $I_0 = 1 \times 10^{14}$ W/cm^2, where n_c is the critical density of the 3ω laser. The physics behind the distributions are very similar for SBS, so we take cases of SRS as examples and leave discussions on SBS until later.

The 100 kJ laser facility[19] is used here for discussion. The laser configuration is shown in Figure 1. There are 48 beams in total delivering a maximum 180 kJ energy. The beams are incident on four cones of different angles relative to the hohlraum axis: 28.5° (8 beams), 35° (8 beams), 49.5° (16 beams) and 55° (16 beams). In Figure 1, we project the beam ports on the whole spherical surface onto a polar coordinates in two dimensions using the Lambert azimuthal equal-area projection. These beam ports are shown in black rectangles with an equal area, and stretch to a narrow region as we plot the beam ports on the other hemisphere. The original polarization configuration of the 100 kJ laser facility is that half beams are s-polarized and the other half are p-polarized. The polarization direction of these beams can turn 90° using an optical rotation crystal if needed; therefore, in this theoretical paper we arbitrarily changed the polarization of the beam and chose any beam from the facility. Here the used beam would be colored in green or blue, representing an s-polarized laser and a p-polarized laser, respectively. The definition of the s-polarization direction is perpendicular to the plane of incidence, containing the incident direction and the pole axis of the sphere, and the p-polarization direction is in that plane.

The growth rate of multibeam instability is the imaginary part of the solution (frequency) of Equation (5) as a function of the wave vector, $\gamma = \gamma(\vec{k}) = \text{Im}(\omega)$. What we care about is the three-dimensional distribution of the growth rate with respect to the scattered light wave vector, that is, $\gamma = \gamma(\vec{k}_s)$, where $\vec{k}_s = \vec{K}_{0i_0} - \vec{k}$. Since the wave number of the scattered wave is defined by the condition of the maximum growth rate, we rewrite the growth rate as a function of the polar angle θ_0 and azimuthal angle ϕ_0, $\gamma = \gamma(\theta_0, \phi_0)$, where θ_0 and ϕ_0 are quantities in vacuum. The three-dimensional sphere is projected to a 2D circle via the Lambert azimuthal equal-area projection, as shown in the following Figures 1–6, where the spokes show the azimuthal angle and the rings show the polar angle.

Figure 1 shows the distribution of the single-beam growth rate. The green rectangle denotes the s-polarized incident beam and the blue rectangle denotes the p-polarized incident beam. The theoretical single-beam growth rate predicts that the maximum growth mode is backscattering with $\gamma_0 = 7.478 \times 10^{-4}\omega_0^{-1}$ under the given parameters. Both Figures 1(a) and 1(b) show that the most unstable growing direction is backward (right at the incident beam), and the growth rate $\gamma_{bs} = 7.474 \times 10^{-4}\omega_0^{-1}$ agrees with the theoretical result. In addition, we find that the distribution prefers to occur out of the plane of polarization due to polarization coupling. This could be a basic criterion to understand more complicated distributions due to multiple beam polarization coupling, as will be shown below.

3.2. *Two-beam interactions*

In a single-beam instability, backscattering is always the most unstable mode in homogeneous plasmas due to its largest wave number being that of the plasma wave; however, it is not always true for multibeam instabilities. Here we will show several distributions of growth rates under two, four and eight beams, and try to find the rules that govern the multibeam physics. Most of the time the maximum growth rate is that of some special modes, such as the SL mode, SP mode or (near) backward mode; these modes have received the most attention in our discussions.

Firstly, let us focus on the two-beam instability in this section. Each beam could either be s-polarized or p-polarized; therefore, there are four possibilities in total. Theoretically,

https://doi.org/10.1017/hpl.2025.10037 Published online by Cambridge University Press

Table 1. Average polarization factor $\langle\cos^2\phi\rangle$ ($\langle\cos^2\phi\rangle = \frac{1}{N}\sum_{j=1}^{N}\cos^2\phi_{0j}$) of the SL mode and SP mode under different polarization configurations. The black, red and green arrows in the insets represent the wave vectors of incident lights, scattered lights and plasma waves, respectively.

Configuration	SL mode 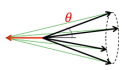	SP mode 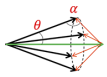
S	1	1
P	$\cos^2\theta$	$\cos^2\alpha$
S-P	1/2	$(1+\cos^2\alpha)/2$
S/8S	1/2	1
P/8P	$\cos^2\theta/2$	$\cos^2\alpha$
S-P-S-P	$(1+\cos^2\theta)/2$	$(1+\cos^2\alpha)/2$
S–2P/4S–4P	$(1+\cos^2\theta)/4$	$(1+\cos^2\alpha)/2$

we could obtain the growth rates of the SL mode and SP mode via Equations (8) and (10). The critical point is the polarization factor. Table 1 summarizes the average polarization factor, $\langle\cos^2\phi\rangle = \frac{1}{N}\sum_{j=1}^{N}\cos^2\phi_{0j}$, under different conditions. For two s-polarized beams, both the SL mode and SP mode have $\langle\cos^2\phi\rangle = 1$; therefore, we have the following:

$$\gamma^2_{\mathrm{SL,2S}} = \frac{k^2_{\mathrm{SL}}v_0^2}{8}\frac{\omega_{\mathrm{pe}}}{\omega_0-\omega_{\mathrm{pe}}},$$
$$\gamma^2_{\mathrm{SP,2S}} = \frac{k^2_{\mathrm{SP}}v_0^2}{8}\frac{\omega_{\mathrm{pe}}}{\omega_0-\omega_{\mathrm{pe}}}. \tag{11}$$

Since the plasma wave number of the SL mode is larger than that of the SP mode (shown in green arrows in the insets of Table 1), we have $\gamma_{\mathrm{SL}} > \gamma_{\mathrm{SP}}$, so the SP mode will not dominate here. For the backward SRS, we already have $\gamma_0^2 = \frac{k^2_{\mathrm{bs}}v_0^2}{16}\frac{\omega_{\mathrm{pe}}}{\omega_0-\omega_{\mathrm{pe}}}$ in the single-beam situation. Although it has the largest wave number k_{bs}, it still needs to compensate a factor of $\sqrt{2}$ to overtake the SL mode, so γ_{SL} will usually be larger than γ_{bs} unless the incidence angle is very small.

Figure 2 shows growth rate distributions of two s-polarized beams for four different incidence angles. The green rectangles denote the s-polarized beams, while the bold one is the specific i_0 beam. The asymmetric nature of the distribution is due to the use of a specific beam; if the other beam is simulated, the whole picture would be obtained. However, the beams are symmetrical in this case, so we will not plot such distributions. As we can see from the figures, the

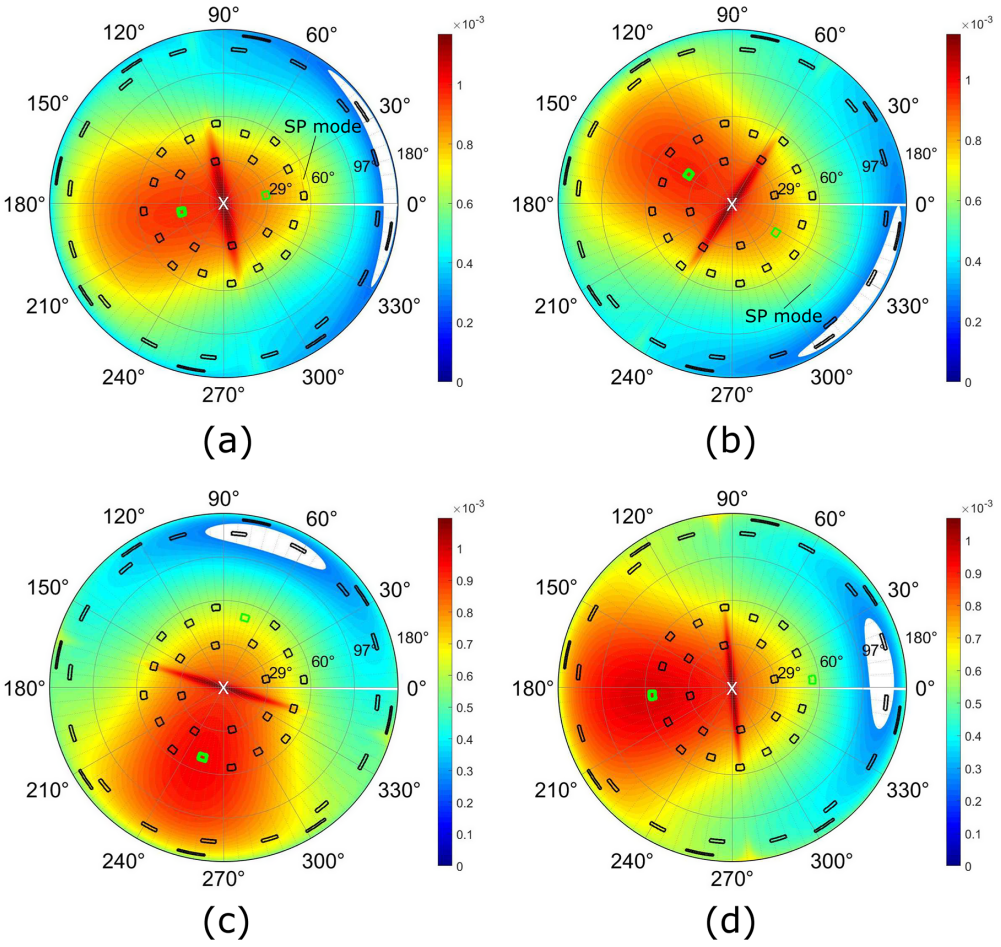

Figure 2. Distributions of growth rates of two s-polarized beams (green rectangles) under four incidence angles: (a) 28.5°, (b) 35°, (c) 49.5° and (d) 55°. The resonant beam is shown with a bold rectangle. The modes with the maximum growth rate are marked by a white 'X'.

https://doi.org/10.1017/hpl.2025.10037 Published online by Cambridge University Press

Table 2. A summary of the maximum growth rates under different polarization configurations when $\theta_0 = 49.5°$ (denoted by 'Maximum'). The growth rate of a backward scattered seed whose polarization is aligned with the resonant beam is also evaluated under the same conditions (denoted by 'Backward').

Configuration	2S	2P	S-P	P-S	4S	4P	S-P-S-P	S-S-P-P	8S	8P	4S-4P
Maximum ($\times 10^{-4}\omega_0^{-1}$)	11.0	8.3	8.4	9.6	11.0	10.4	12.4	10.3	14.7	11.8	12.4
Backward ($\times 10^{-4}\omega_0^{-1}$)	9.7	8.3	8.3	9.6	9.2	9.3	9.8	8.9	9.4	9.9	9.4

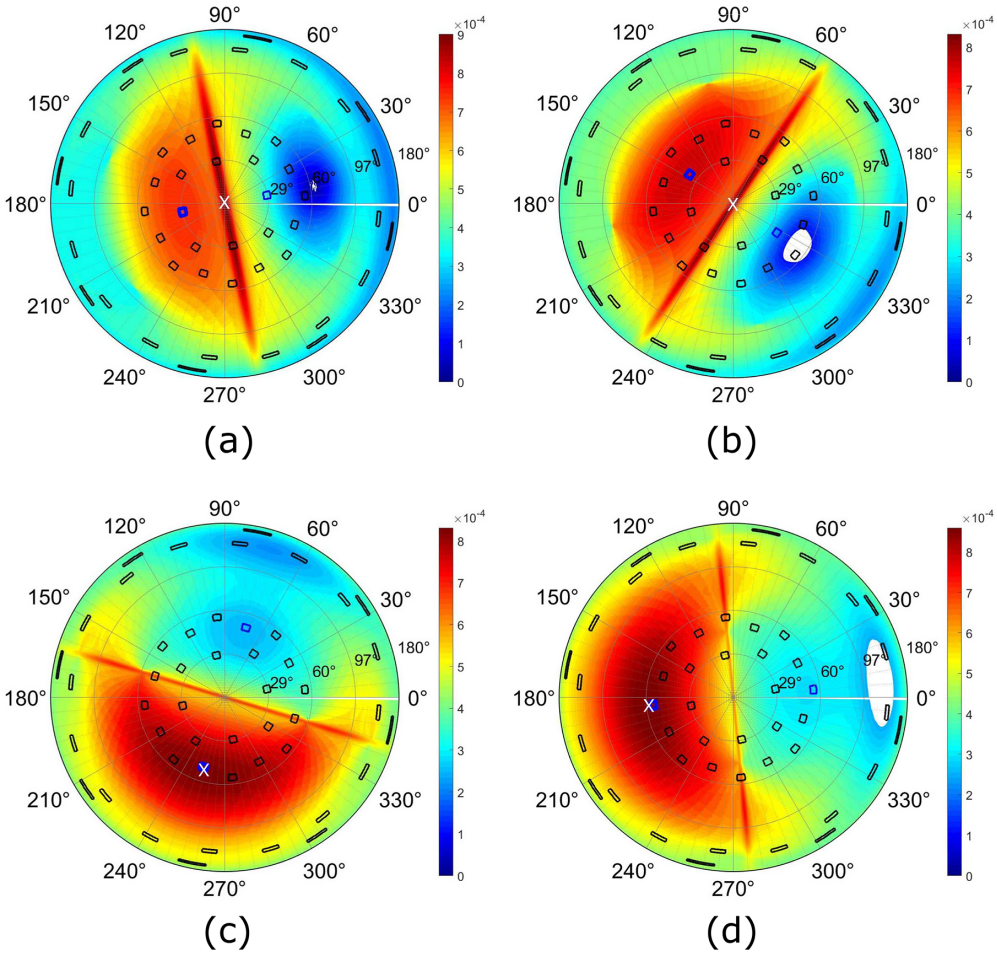

Figure 3. Distributions of growth rates of two p-polarized beams (blue rectangles) under four incidence angles: (a) 28.5°, (b) 35°, (c) 49.5° and (d) 55°.

brightest lines in red in the center of two beams are the SL modes, which are the bisector of two beams[18]. The most unstable mode denoted by a white X is the exact backward SL mode, and its growth rate satisfies the theoretical result, $\gamma_{\max} = 1.1 \times 10^{-3}\omega_0^{-1} \approx \gamma_{\mathrm{SL}}$. The SP mode depicted by thin curves, as shown in Figure 2(a), however, is rather weak. As the incidence angle increases, the SP mode becomes weaker and weaker, and it will disappear when half of the intersection angle, which is also the incidence angle θ_0 here, is higher than 37.4°[14], as shown in Figures 2(c) and 2(d).

We also note that the growth rate of backward scattering is enhanced by multibeam interactions, from $\gamma_0 = 7.478 \times 10^{-4}\omega_0^{-1}$ to $\gamma_{\mathrm{bs}} \approx 9.7 \times 10^{-4}\omega_0^{-1}$. This leads to another question regarding the multibeam system: what is the growth rate of a backward seed in the multibeam region and would it be comparable to the maximum growth rate of a noise seed? We evaluate such circumstances in Table 2 for different cases. In very few cases, the growth rate of a backward seed is dominant in the multibeam regions, which will be discussed soon. Most of the time the multibeam modes overtake the backward scattering. One more thing we find in Figure 2 is that as the incidence angle increases the maximum growth rate decreases (as the SL mode decreases); however, backward or near backward modes do not. This may lead to the transition of dominant modes as the incidence angle changes.

Figure 3 shows the growth rates under two p-polarized beams (blue rectangles). The average polarization factor is

https://doi.org/10.1017/hpl.2025.10037 Published online by Cambridge University Press

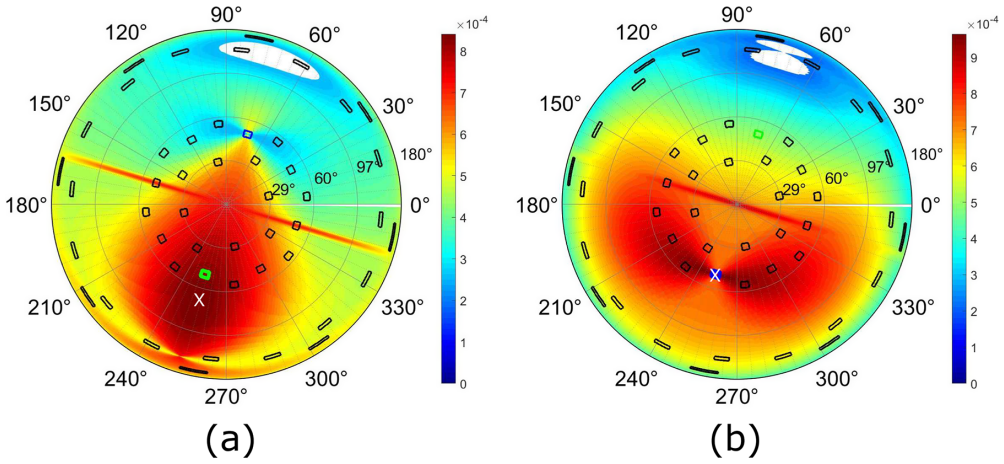

Figure 4. Distributions of growth rates of an s-polarized beam (green rectangle) and a p-polarized beam (blue rectangle): (a) the resonant beam is s-polarized (S-P interactions), while (b) the resonant beam is p-polarized (P-S interactions).

$\langle\cos^2\phi\rangle = \cos^2\theta$ for the SL mode and $\langle\cos^2\phi\rangle = \cos^2\alpha$ for the SP mode, so we have the following:

$$\gamma^2_{\mathrm{SL,2P}} = \frac{k^2_{\mathrm{SL}}v_0^2}{8}\frac{\omega_{\mathrm{pe}}}{\omega_0-\omega_{\mathrm{pe}}}\cos^2\theta,$$
$$\gamma^2_{\mathrm{SP,2P}} = \frac{k^2_{\mathrm{SP}}v_0^2}{8}\frac{\omega_{\mathrm{pe}}}{\omega_0-\omega_{\mathrm{pe}}}\cos^2\alpha, \qquad (12)$$

where α is the angle between the incident and scattered wave vectors, as shown in the insets of Table 1. This angle is close to 90° ($\alpha = 94.4°$ for $\theta_0 = 28.5°$), so $\gamma_{\mathrm{SP,2P}}$ is pretty small. The relationship between the SL mode and (near) backward scattering depends on the incidence angle. Backward scattering will dominate in the 2P system when the incident angle is large.

Figure 3 represents such interactions. When $\theta_0 = 29.5°$ and 35° (shown in Figures 3(a) and 3(b)), the backward SL mode is the most unstable mode. The growth rate of the SL mode decreases with the angle drastically, while the growth rate of backward scattering is slightly increased, so the dominant mode changes to (near) backward scattering as $\theta_0 \geq 49.5°$. The maximum growth rate of the 2P system is also not very large, $\gamma_{\max} \approx (8-9)\times 10^{-4}\omega_0^{-1}$, implying the inefficiency of the p-polarized beam in constructing multibeam modes. Since $\cos^2\alpha < \cos^2\theta$ for incidence angles that are not too small, the SP mode will not dominate in this case, either.

The last two cases are the combination of an s-polarized beam and a p-polarized beam. The polarization directions of these two beams are perpendicular to each other, so one would expect an inefficient coupling of two beams. The average polarization factors are $\langle\cos^2\phi\rangle = 1/2$ for the SL mode and $\langle\cos^2\phi\rangle = (1+\cos^2\alpha)/2$ for the SP mode, which makes their growth rate as follows:

$$\gamma^2_{\mathrm{SL,S-P}} = \frac{k^2_{\mathrm{SL}}v_0^2}{16}\frac{\omega_{\mathrm{pe}}}{\omega_0-\omega_{\mathrm{pe}}},$$
$$\gamma^2_{\mathrm{SP,S-P}} = \frac{k^2_{\mathrm{SP}}v_0^2}{16}\frac{\omega_{\mathrm{pe}}}{\omega_0-\omega_{\mathrm{pe}}}\left(1+\cos^2\alpha\right), \qquad (13)$$

with the same factor 1/16 with backscattering. Compared with backward scattering, it is easy to find that $\gamma_{\mathrm{bs}} > \gamma_{\mathrm{SL}}$ and γ_{bs} will always be larger than γ_{SP}.

Figure 4 shows typical cases of 49.5° of (Figure 4(a)) S-P and (Figure 4(b)) P-S interactions, where the first letter denotes the resonant beam. As shown, (near) backward scattering dominates the S-P or P-S system as we expect from theoretical analysis. However, the distributions on the s-side are a little different from those on the p-side. The mode with the maximum growth rate on the s-side slightly drifts away from the exact backward direction as the incidence angle increases, and its growth rate also increases. A probable explanation for the phenomenon is that a new mode emerges from the combination effect of the single-beam and SL mode on the s-side. Meanwhile, on the p-side, the maximum is exactly the backward scattering no matter what the incidence angle is. Its growth rate reaches as high as $9.6\times 10^{-4}\omega_0^{-1}$, which is higher than that of the s-side. This implies a different growth triggered by differently polarized beams in the multibeam system.

3.3. *Four-beam interactions*

Complexity grows exponentially as the number of incident beams increases. The results obtained from few beams are usually not appropriate for situations with more beams; however, we could still look for some general rules for multibeam interactions. For the four-beam interactions discussed in this section, we concentrate on four polarization combinations: four s-polarized beams (4S), four p-polarized beams (4P), the maximum coupling case (S-P-S-P) and half-s-half-p (S-S-P-P or 2S-2P). The four beams are symmetrically distributed.

https://doi.org/10.1017/hpl.2025.10037 Published online by Cambridge University Press

Four s-polarized beams are perhaps the simplest case of all. We still first discuss the theoretical growth rates of some special modes to estimate a general view of this multibeam system. The average polarization factors for the SL mode and SP mode are 1/2 and 1, respectively. These give the formulas for four s-polarized beams:

$$\gamma^2_{\mathrm{SL,4S}} = \frac{k^2_{\mathrm{SL}} v_0^2}{8} \frac{\omega_{\mathrm{pe}}}{\omega_0 - \omega_{\mathrm{pe}}},$$
$$\gamma^2_{\mathrm{SP,4S}} = \frac{k^2_{\mathrm{SP}} v_0^2}{4} \frac{\omega_{\mathrm{pe}}}{\omega_0 - \omega_{\mathrm{pe}}}. \quad (14)$$

Since the SP mode shares a common plasma wave, each scattered light could couple with its incident light individually, and the coupling factor is always maximized. From then on the SP mode could become enhanced, or even dominant under specific conditions. Owing to the increasing beam number, the multiplier increases as $\gamma \propto \sqrt{N}$, so backward scattering is less likely to be observed as the dominant mode. This has been verified in Table 2. The order of γ_{SL} and γ_{SP} depends on the laser–plasma conditions, but both of them are always larger than γ_{bs}. Interestingly, the growth rate of the SL mode in the 4S system is the same as that in the 2S system, $\gamma_{\mathrm{SL,2S}} = \gamma_{\mathrm{SL,4S}}$.

Distributions of four s-polarized beams are shown in Figures 5(a) and 5(c). For $\theta_0 = 28.5°$ in Figure 5(a), both the SL mode and SP mode are observed. The SL modes are shown to occur at the bisector of four incident waves (denoted by the large cross), where the four incident waves can share a common scattered light, and the maximum growth rate is located at the center, which is the exact backward SL mode. We also find the maximum growth rate is coincident with that in the 2S system. The SP modes shown by thin curves are, however, not the dominant mode. This is because the joint effect of the single-beam interaction and SL mode is much more efficient than that of the SP mode. As θ_0 increases to 49.5°, as shown in Figure 5(c), the SP mode becomes weaker. The SP mode will dominate at smaller incidence angles, such as for beams in quads of the National Ignition Facility (NIF)[21] or Shenguang Octopus facility[16].

Four p-polarized beams are the least coupling combination of all. The average polarization factors are $\cos^2\theta/2$ for the SL mode and $\cos^2\alpha$ for the SP mode. Then the growth rates are given by the following:

$$\gamma^2_{\mathrm{SL,4P}} = \frac{k^2_{\mathrm{SL}} v_0^2}{8} \frac{\omega_{\mathrm{pe}}}{\omega_0 - \omega_{\mathrm{pe}}} \cos^2\theta,$$
$$\gamma^2_{\mathrm{SP,4P}} = \frac{k^2_{\mathrm{SP}} v_0^2}{4} \frac{\omega_{\mathrm{pe}}}{\omega_0 - \omega_{\mathrm{pe}}} \cos^2\alpha. \quad (15)$$

Obviously $\gamma_{\mathrm{SL,4P}} < \gamma_{\mathrm{SL,4S}}$ and $\gamma_{\mathrm{SP,4P}} < \gamma_{\mathrm{SP,4S}}$. However, it is difficult to tell which mode will dominate until we have evaluated them, so the order of γ_{SL}, γ_{SP} and γ_{bs} depends on particular conditions.

Figures 5(b) and 5(d) show the distribution of 4P cases when $\theta_0 = 28.5°$ and 49.5°, respectively. In Figure 5(b), apart from the cross-shaped bisector of the SL mode, the most prominent SL mode is the line in the center, which perpendicularly bisects the resonant beam and its opposite beam. It is this new mode that gives a chance that the SP mode can be resonant with the SL mode, and the intersection point of the two special modes dominates in this case, as shown by white 'X' in Figure 5(b). As the incidence angle increases to 49.5°, both SP modes and center SL modes weaken. The SL modes bisected by the resonant beam and its nearby beam become stronger, and their combination with the single-beam interaction contributes to the maximum growth rates, as denoted by white 'X' in Figure 5(d). One could find that for a multibeam system the maximum growth rate could not only be an SL mode, (near) backward scattering, but be other directions as well.

For a more complex polarization configuration, the distribution of the growth rate could be intricate. Here we discuss the cases of S-P-S-P and S-S-P-P and plot their distributions when $\theta_0 = 49.5°$ in Figures 5(e) and 5(f), respectively. In Figure 5(e), since the incident beams are symmetric to the resonant beam, the distribution is also symmetric with that beam. The SL mode in the center dominates the case. The S-P-S-P case is also the strongest coupling case, as all beams have the maximum components in one direction, say the direction of the s-polarized beam. The growth rate is also the highest of all. For the S-S-P-P case, which is also the real polarization configuration in the 100 kJ laser facility, the distribution in Figure 5(f) shows that the growth rate is asymmetric due to asymmetric incident beams. The maximum growth rate is also non-axial and non-backward; it is along the bisector of the s-polarized beam and p-polarized beam and results from both SL mode and single-beam interaction.

3.4. Eight-beam interactions

Finally, let us take a look at the eight-beam interaction, which is usually the maximum beam/quad number of a cone in many laser facilities, such as the NIF and the 100 kJ laser facility discussed here. We choose three polarization combinations: all s-polarized beams, all p-polarized beams and half-s-half-p beams. As shown in Table 1, the average polarization factors are the same as the corresponding four beam cases; therefore, we expect that the physics will remain the same.

Figure 6 shows the distributions of eight-beam interactions under various conditions. First of all, the backward scattering is further out of dominance. The discrepancy between the backward scattering and the true multibeam mode with

https://doi.org/10.1017/hpl.2025.10037 Published online by Cambridge University Press

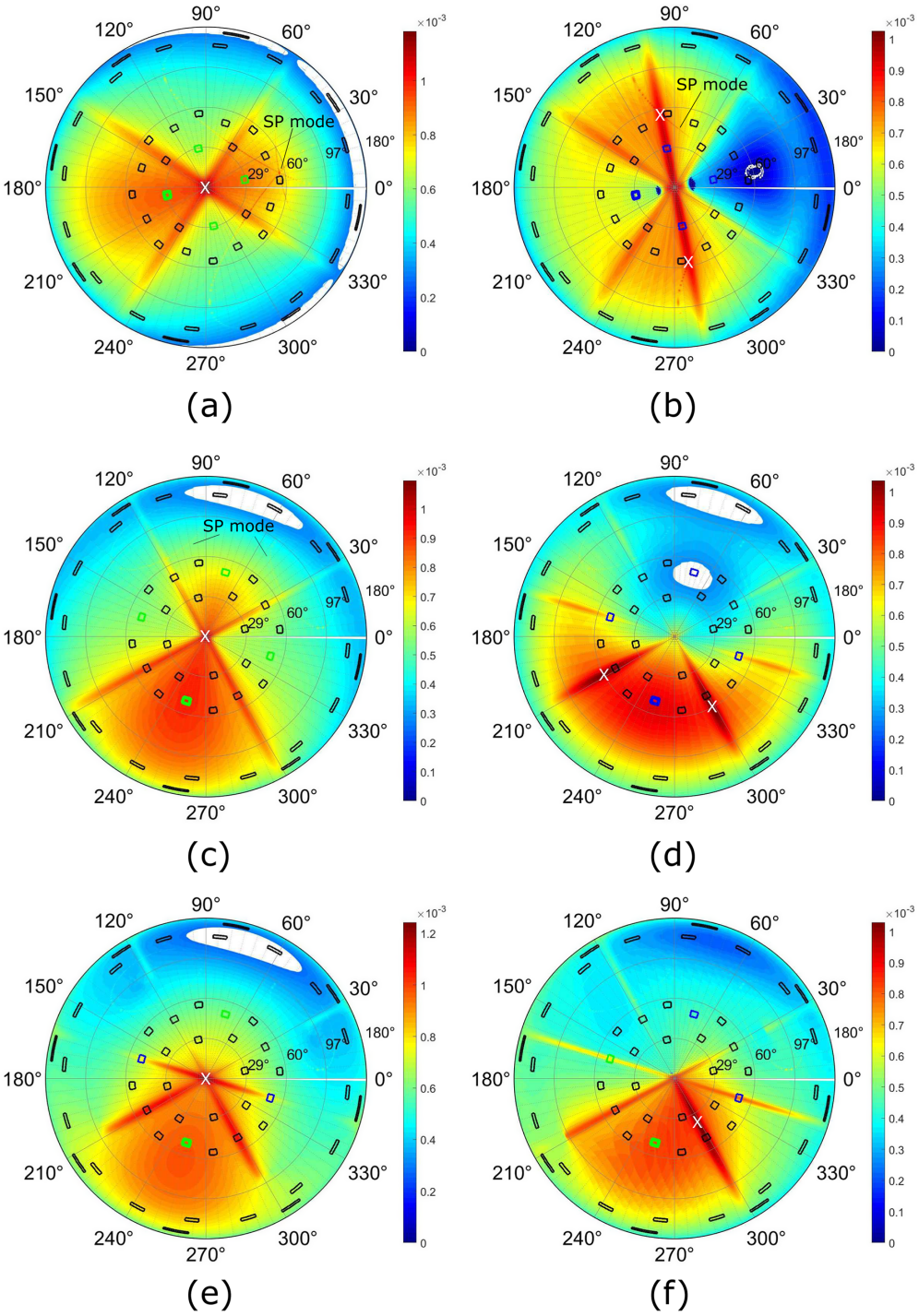

Figure 5. Distributions of growth rates of four incident beams: (a)–(f) are varied in polarization configurations and incident angles as depicted in each plot.

the maximum growth rate is becoming larger, as shown in Table 2.

Specifically, let us discuss the case of 8S first. Figure 6(a) uses two inner cones as incident beams. The SL mode in the center is the dominant mode. We find that the distributions are more localized, especially along the two bisectors between the resonant beam and its nearest beams. The SP mode is weak here, owing to fewer interactions with other special modes. We find that when the incidence angle is very small, such as a few degrees, the SP mode would be dominant in the multibeam system. As for the 8P cases shown in the second row, the physics is very similar to that in the 4P cases. The two symmetric growth rates along the nearest bisectors dominate those cases. Many spoke-shape

https://doi.org/10.1017/hpl.2025.10037 Published online by Cambridge University Press

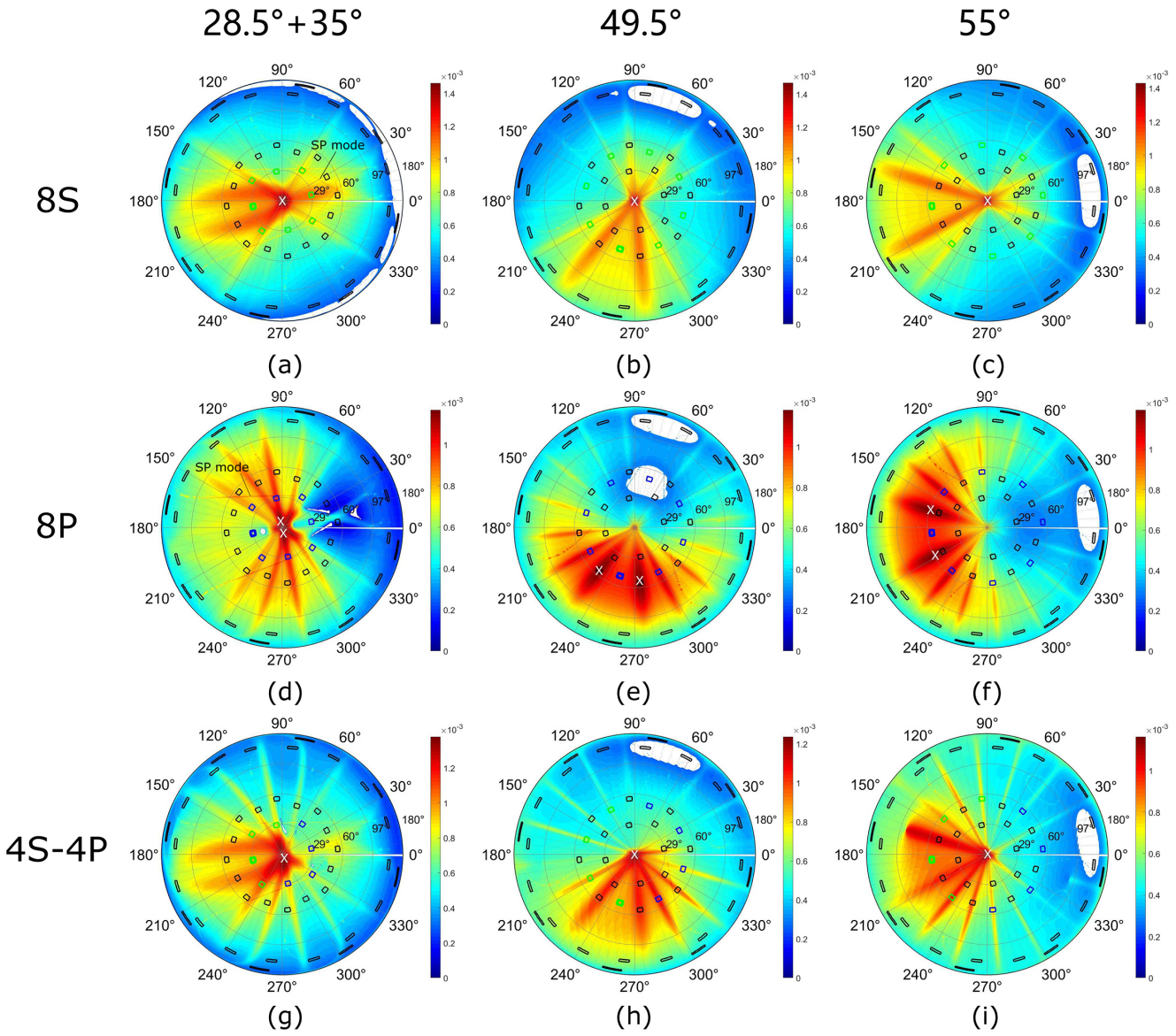

Figure 6. Distributions of growth rates of eight incident beams: (a)–(i) are varied in polarization configurations and incidence angles as described in the top and left.

distributions along the bisectors and incident beams are a characteristic of p-polarized beams. In the case of half-s-half-p, the asymmetric mode dominates the distribution; however, since it includes a large number of s-polarized beams, the exact backward SL mode dominates the system.

4. An inference of general rules that govern the growth of multibeam systems

SRS and SBS are similar LPIs in that an incident electromagnetic wave decays into a scattered electromagnetic wave and an electrostatic plasma wave. The physics of instability growth in the multiple beam overlapping region shares similar features. We have also calculated distributions of SBS growth rates under various conditions and found that the behaviors of the maximum growth rate, SL mode, SP mode and backward scattering look the same with SRS. The differences are only in the magnitude of the growth rate and the spread width of those modes. However, if the frequencies of incident beams change a little, the multibeam mode of SBS changes dramatically due to the tinny frequency of the ion acoustic wave. This could give rise to CBET. For SRS, a slight frequency change will barely affect the distribution. This effect is not the purpose of this paper.

From the above analyses of the effect of a few beam and polarization configurations on the growth rate distribution, we can infer some general rules that govern the growth of multibeam systems.

(1) Backward scattering: when the beam number is larger than four, backward scattering will not be the

https://doi.org/10.1017/hpl.2025.10037 Published online by Cambridge University Press

dominant mode anymore. If the beam number is large enough and the beams are distributed equally or randomly in a closed curve, an expectation of the average polarization factor is supposed to be 1/2. Therefore, the multibeam mode, such as the SL mode or SP mode, readily exceeds the growth rate of backscattering when $N \geq 4$. Although we find that the growth rate of the backscattering seed in multibeam region would be enhanced relative to a single beam, the enhancement is negligible compared with other multibeam modes. For $N = 2$ or 3, the dominant mode should be carefully analyzed according to specific laser–plasma conditions.

(2) SL mode: the structure of the SL mode is the most common feature in the distribution of growth rates as seen from the scattered light perspective. It occurs at the bisector of any two beams, but prefers those near the resonant beam. The most important SL mode is the one along the symmetric axis, that is, at the center of our plot. We infer that when s-polarized beams are dominant, this SL mode is always the most unstable mode, since its average polarization factor is always higher than 1/2 and the plasma wave number is dominant over the SP mode, $k_{SL} > k_{SP}$. The SL-dominant case would be the most common case observed in the multibeam overlapping region, except for some extreme cases, such as when the incident angle is too small or too large.

(3) SP mode: the subdominancy of the SP mode is due to its small plasma wave number; however, this subdominancy could also convert to dominancy under particular conditions. The advantage of the SP mode is its high coupling efficiency, since each scattered light could couple with its corresponding incident light. The polarization factor is 1 for an s-polarized beam and $\cos^2\alpha$ for a p-polarized beam; therefore, the SP mode prefers a small incidence angle (large $\cos^2\alpha$) and an environment with more p-polarized beams (less efficient for the SL mode). The direction of scattered light from the pure SP mode is opposed to the incident beam.

(4) Other multibeam modes: these modes occur neither along the polar axis nor the backward or opposed direction to the incident beam. They are often a combination of two or three special modes discussed above. These modes are often seen in the less-efficient coupling case (such as all p-polarized beams) and asymmetrically distributed case (perhaps with an equal number of s-polarized and p-polarized beams). The SL mode is a core to connect the backscattering and SP mode, so we can always observe such modes along the bisector of certain cases of two beams.

5. Spatial distributions obtained from particle-in-cell simulations

To verify the reduced model, we have performed 2D PIC simulations of SRS with two crossing laser beams using EPOCH code. A three-dimensional PIC simulation of more beams is time-consuming, so it is not presented in this paper. The spatial distributions of scattered light characterized by angular distribution in the plane of incidence are plotted in Figure 7.

The simulation setup is similar to our previous paper[12]. Two laser beams with the same intensity $I = 1 \times 10^{15}$ W/cm^2 are incident into a uniform plasma $n_e = 0.14 n_c$. The incidence angle is varied from 49° to 58° in vacuum, correspondingly 45° to 55° in plasma. Two beams are either two s-polarized (polarized along the z-axis) or one s-polarized and the other p-polarized (polarized in the $x-y$ plane). Other parameters include electron temperature $T_e = 2$ keV, ions are fixed to form a neutral background and the total simulation time is 1.5 ps. The simulation box is 40 μ m(x) × 10 μm (y) with 6000 and 1500 grids on each side, and 30 particles in each cell. Four boundaries are all set to be open in order to exclude unphysical transverse amplification, and thermal particle boundaries are used. The two beams overlap in the center of the simulation box and excite multibeam instabilities.

The time-averaged field spectra in the overlapping region are shown in Figure 7. The left-hand column shows the longitudinal field spectra, the middle column shows the transverse field spectra and the right-hand column shows the corresponding spatial distributions of scattered light. Two types of spatial distributions are shown here: the red and green curves are interpolated from the dispersion relation on the longitudinal field spectra (left), and blue or magenta dotted curves are interpolated from the dispersion relation on the transverse field spectra (middle or left). As we can see, the two metrics of scattered light spectra seem to have little difference in shape. For the metric of longitudinal spectra (solid curves), the two spatial distributions are nearly the same for the two s-polarized beams in the first two rows. For the s-p combination shown in the third row where the upper beam is p-polarized and lower beam is s-polarized, the spectra differ both in shape and amplitude. The scattered amplitude of the p-polarized beam (polarized in the $x-y$ plane) is stronger and its spectral width is narrower than that of the s-polarized beam (polarized along the z-axis), which is consistent with Figure 4 from the reduced model.

The collective mode excited by the two overlapping beams is also apparent. For two s-polarized beams, the dominant mode is the SL mode propagating along the symmetry axis where the polar angle is 0. This mode is away from the backscattering indicated by black-dashed lines in Figures 7(c) and 7(f). As we change the upper beam from s-polarization to p-polarization, the dominant mode changes

https://doi.org/10.1017/hpl.2025.10037 Published online by Cambridge University Press

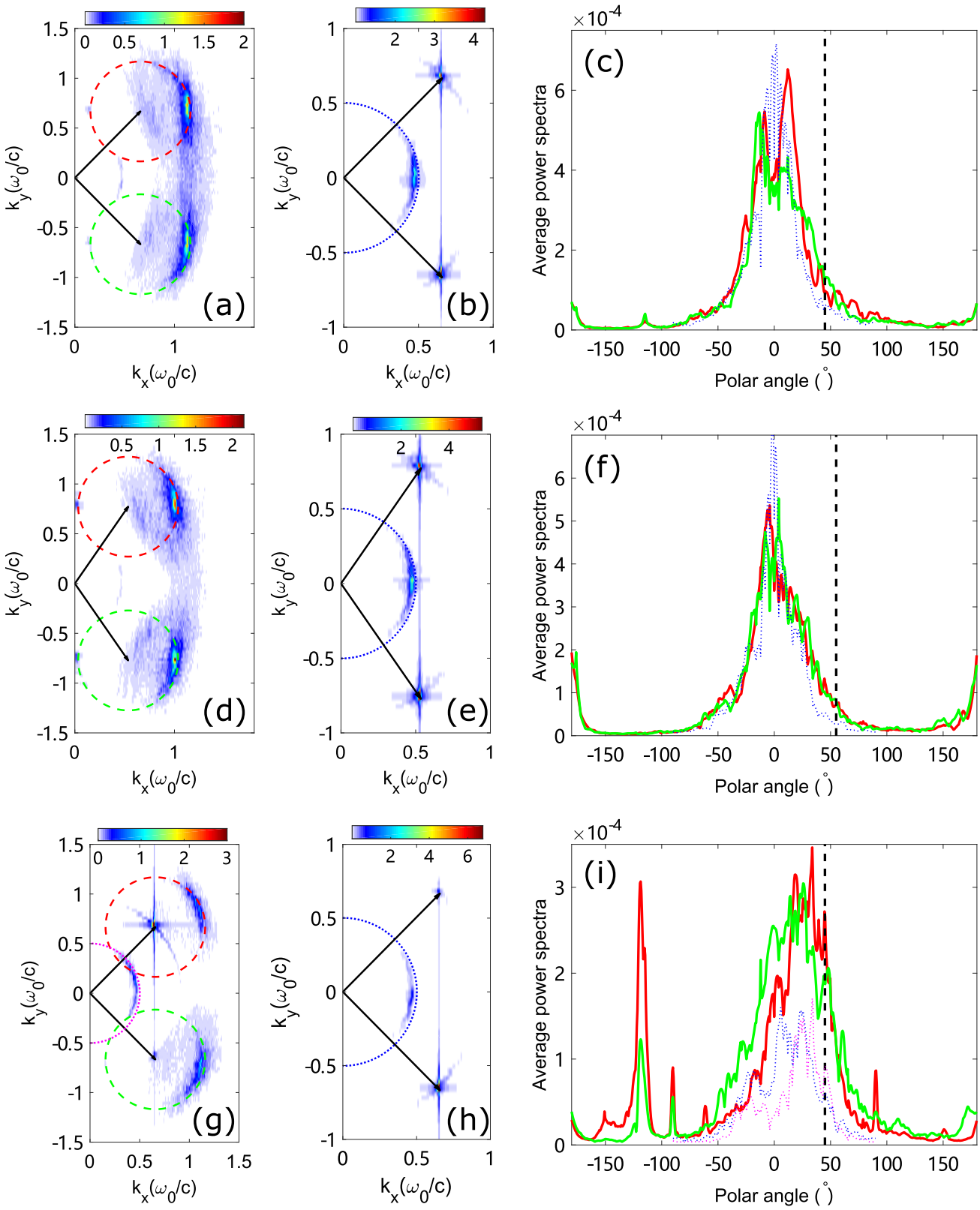

Figure 7. Particle-in-cell simulations of two-beam SRS in two-dimensions. The left-hand and middle columns show the time-averaged longitudinal and transverse field spectra, respectively: two s-polarized beams incident with (a) $\theta = 45°$, (d) $\theta = 55°$, and a p-polarized beam (upper) and an s-polarized beam (lower) incident with (g) $\theta = 45°$. The figures in the right-hand column are the corresponding spatial distributions of scattered light, which are interpolated along circles in the left-hand figures. The center ($\theta = 0°$) indicates scattered light along the $-x$ direction.

https://doi.org/10.1017/hpl.2025.10037 Published online by Cambridge University Press

to near backscattering, as shown in Figure 7(i). These results are qualitatively consistent with Figures 2 and 4, showing good agreement between the reduced model and PIC simulations.

The reduced model is based on the assumption that the laser beam is monochromatic and the plane wave and plasma are homogeneous. It is also a linear analysis of the wave coupling equations. In the PIC simulations, we find that although nonlinear phenomenon (here the nonlinear frequency shift[12]) occurs, the main physics that the SL mode is dominant still remains. For more realistic conditions, new modes such as side scatterings in inhomogeneous plasma would compete with the multibeam modes, and laser speckles, which introduce a spread on the incidence angles, also affect the spectrum of the multibeam mode. The reduced model could be easily extended to include multicolor incident beams, allowing the description of the effect of CBET, but the broadband laser is beyond this simple model. Nonlinear phenomena, such as laser filamentation and the kinetic effect, are not included here, and need more detailed kinetic simulations. Therefore, the reduced model could be a quick approach to obtain the linear physics of multibeam instabilities; however, it is also limited in more complex situations. The model verified by PIC simulations could be added into more sophisticated models, such as the ray-tracing model, to extend its application.

6. Conclusions

In this paper, we have obtained a reduced dispersion relation for multibeam LPIs, which is easily turned into numerical calculations. The dispersion relation consists of three main effects: self-coupling, SL modes and SP modes. Then we solve the dispersion relation numerically under various beam numbers, configurations and polarizations in order to understand the physics of multibeam instability with general conditions. The growth of instability in the beam overlapping region is complicated; however, a few general results could be deduced, such as the dominancy of the SL mode and the subdominancy of backscattering and the SP mode. The 2D PIC simulation results also show good agreement with the reduced model. The dispersion relation provides us with a strong tool to deeply excavate the instability in the overlapping region, which has not been done before.

Appendix. Dispersion relation with respect to scattered light

All the dispersion relations discussed above, from Equations (1)–(5), are derived in the reference frame of a plasma wave, and then we change the frame to scattered light near the specific beam i_0 to get the spatial distribution of scattered light. Alternatively, we can derive the dispersion relations for scattered light directly. It will be shown that all we need to do is to change the coefficient μ_k^{ij}. By repeating the first steps of our previous theoretical paper[18], the coupling equation for complex scattered light amplitude $\widehat{a}_s$ is given by the following:

$$D_l\left(\vec{k},\omega\right)\widehat{a}_s\left(\vec{k},\omega\right)=\Gamma_0^2\sum_{i=1}^{N}\frac{\left|\vec{k}-\vec{K}_{0i}\right|^2\cos\phi_{0i}}{D_p\left(\vec{k}-\vec{K}_{0i},\omega-\omega_0\right)}\times\sum_{j=1}^{N}\widehat{a}_s\left(\vec{k}-\Delta\vec{K}_{ij},\omega\right)\cos\phi_{0j}, \tag{16}$$

where D_l and D_p are the light wave and plasma wave dispersion functions, respectively, $\vec{K}_{0i}$ is the wave vector of the pump laser, $\Delta\vec{K}_{ij}=\vec{K}_{0i}-\vec{K}_{0j}$, $\vec{k}$ and ω are the wave vector and frequency of scattered light, respectively, and Γ_0 and $\cos\phi$ are as defined previously. Equation (16) could be transformed into another form:

$$\epsilon_0\left(\vec{k},\omega\right)\widehat{a}_s\left(\vec{k},\omega\right)=\sum_{i=1}^{N}\left[\sum_{j=1,j\neq i}^{N}\epsilon_{ij}\left(\vec{k},\omega\right)\widehat{a}_s\left(\vec{k}-\Delta\vec{K}_{ij},\omega\right)\right], \tag{17}$$

where

$$\epsilon_0\left(\vec{k},\omega\right)=D_l\left(\vec{k},\omega\right)-\Gamma_0^2\sum_{i=1}^{N}\left[\frac{\left|\vec{k}-\vec{K}_{0i}\right|^2\cos^2\phi_{0i}}{D_p\left(\vec{k}-\vec{K}_{0i},\omega-\omega_0\right)}\right], \tag{18}$$

$$\epsilon_{ij}\left(\vec{k},\omega\right)=\frac{\left|\vec{k}-\vec{K}_{0i}\right|^2\Gamma_0^2\cos\phi_{0i}\cos\phi_{0j}}{D_p\left(\vec{k}-\vec{K}_{0i},\omega-\omega_0\right)}. \tag{19}$$

Therefore, the coupling equation can be rewritten to a simplified form:

$$a_k=\sum_{i=1}^{N}\left(\sum_{j=1,j\neq i}^{N}\mu_k^{ij}a_{k-\Delta K_{ij}}\right), \tag{20}$$

which is just Equation (8) in Ref. [18], the starting equation for deriving the dispersion relation. The coefficient $\mu_k^{ij}=\epsilon_{ij}(\vec{k},\omega)/\epsilon_0(\vec{k},\omega)$ is a little different from Equation (2) with replacing Equations (18) and (19) in the formula. The reduced dispersion relation for scattered light can be derived accordingly:

$$1=\frac{\left|\vec{k}-\vec{K}_{0i_0}\right|^2\Gamma_0^2\cos^2\phi_{0i_0}}{D_l\left(\vec{k},\omega\right)D_p\left(\vec{k}-\vec{K}_{0i_0},\omega-\omega_0\right)}$$

https://doi.org/10.1017/hpl.2025.10037 Published online by Cambridge University Press

$$+\sum_{j_0=1,j_0\neq i_0}^{N}\frac{\left|\overrightarrow{k}-\overrightarrow{K}_{0i_0}\right|^2\Gamma_0^2\cos^2\phi_{0j_0}}{D_{\mathrm{l}}\left(\overrightarrow{k}-\Delta\overrightarrow{K}_{i_0j_0},\omega\right)D_{\mathrm{p}}\left(\overrightarrow{k}-\overrightarrow{K}_{0i_0},\omega-\omega_0\right)}$$
$$+\sum_{i=1,i\neq i_0}^{N}\frac{\left|\overrightarrow{k}-\overrightarrow{K}_{0i}\right|^2\Gamma_0^2\cos^2\phi_{0i}}{D_{\mathrm{l}}\left(\overrightarrow{k},\omega\right)D_{\mathrm{p}}\left(\overrightarrow{k}-\overrightarrow{K}_{0i},\omega-\omega_0\right)}. \quad (21)$$

Acknowledgement

This work was supported by the Fund of the National Key Laboratory of Plasma Physics (Grant No. 6142A04230103), the Science Challenge Project (Grant No. TZ2024016), the National Natural Science Foundation of China (Grant Nos. 12475237, 12275251 and 12205274) and the Strategic Priority Research Program of the Chinese Academy of Sciences (Grant Nos. XDA25050700 and XDA25010300).

References

1. P. Michel, *Introduction to Laser-Plasma Interactions* (Springer, 2023).
2. J. F. Myatt, J. Zhang, R. W. Short, A. V. Maximov, W. Seka, D. H. Froula, D. H. Edgell, D. T. Michel, I. V. Igumenshchev, D. E. Hinkel, P. Michel, and J. D. Moody, Phys. Plasmas **21**, 055501 (2014).
3. W. L. Kruer, S. C. Wilks, B. B. Afeyan, and R. K. Kirkwood, Phys. Plasmas **3**, 382 (1996).
4. P. Michel, L. Divol, E. A. Williams, S. Weber, C. A. Thomas, D. A. Callahan, S. W. Haan, J. D. Salmonson, S. Dixit, D. E. Hinkel, M. J. Edwards, B. J. MacGowan, J. D. Lindl, S. H. Glenzer, and L. J. Suter, Phys. Rev. Lett. **102**, 025004 (2009).
5. I. V. Igumenshchev, D. H. Edgell, V. N. Goncharov, J. A. Delettrez, A. V. Maximov, J. F. Myatt, W. Seka, A. Shvydky, S. Skupsky, and C. Stoeckl, Phys. Plasmas **17**, 122708 (2010).
6. D. T. Michel, A. V. Maximov, R. W. Short, S. X. Hu, J. F. Myatt, W. Seka, A. A. Solodov, B. Yaakobi, and D. H. Froula, Phys. Rev. Lett. **109**, 155007 (2012).
7. H. X. Vu, D. F. DuBois, D. A. Russell, and J. F. Myatt, Phys. Plasmas **17**, 072701 (2010).
8. J. Zhang, J. F. Myatt, R. W. Short, A. V. Maximov, H. X. Vu, D. F. DuBois, and D. A. Russell, Phys. Rev. Lett. **113**, 105001 (2014).
9. R. K. Follett, J. G. Shaw, J. F. Myatt, D. H. Froula, and J. P. Palastro, Phys. Rev. E **101**, 043214 (2020).
10. G. Cristoforetti, P. Koester, S. Atzeni, D. Batani, S. Fujioka, Y. Hironaka, S. Hüller, T. Idesaka, K. Katagiri, K. Kawasaki, R. Kodama, D. Mancelli, P. Nicolai, N. Ozaki, A. Schiavi, K. Shigemori, R. Takizawa, T. Tamagawa, D. Tanaka, A. Tentori, Y. Umeda, A. Yogo, and L. A. Gizzi, High Power Laser Sci. Eng. **11**, e24 (2023).
11. S. Depierreux, C. Neuville, C. Baccou, V. Tassin, M. Casanova, P.-E. Masson-Laborde, N. Borisenko, A. Orekhov, A. Colaitis, A. Debayle, G. Duchateau, A. Heron, S. Huller, P. Loiseau, P. Nicolaï, D. Pesme, C. Riconda, G. Tran, R. Bahr, J. Katz, C. Stoeckl, W. Seka, V. Tikhonchuk, and C. Labaune, Phys. Rev. Lett. **117**, 235002 (2016).
12. S. J. Yang, H. B. Zhuo, Y. Yin, Z. J. Liu, C. Y. Zheng, X. T. He, and C. Z. Xiao, Phys. Rev. E **102**, 013205 (2020).
13. J. Qiu, L. Hao, L. Cao, and S. Zou, Matter Radiat. Extremes **6**, 065903 (2021).
14. P. Michel, L. Divol, E. L. Dewald, J. L. Milovich, M. Hohenberger, O. S. Jones, L. Berzak Hopkins, R. L. Berger, W. L. Kruer, and J. D. Moody, Phys. Rev. Lett. **115**, 055003 (2015).
15. C. Neuville, V. Tassin, D. Pesme, M.-C. Monteil, P.-E. Masson-Laborde, C. Baccou, P. Fremerye, F. Philippe, P. Seytor, D. Teychenné, W. Seka, J. Katz, R. Bahr, and S. Depierreux, Phys. Rev. Lett. **116**, 235002 (2016).
16. Q. Wang, Z. Li, Z. Liu, T. Gong, W. Zhang, T. Xu, B. Li, P. Li, X. Li, C. Zheng, L. Cao, X. Liu, K. Pan, H. Zhao, Y. Liu, B. Deng, L. Hou, Y. Li, X. Liu, Y. Li, X. Peng, Z. Guan, Q. Wang, X. Che, S. Li, Q. Yin, W. Zhang, L. Xia, P. Wang, X. Jiang, L. Guo, Q. Li, M. He, L. Hao, H. Cai, W. Zheng, S. Zou, D. Yang, F. Wang, J. Yang, B. Zhang, Y. Ding, and X. He, Matter Radiat. Extremes **8**, 055602 (2023).
17. D. F. DuBois, B. Bezzerides, and H. A. Rose, Phys. Fluids B **4**, 241 (1992).
18. C. Z. Xiao, H. B. Zhuo, Y. Yin, Z. J. Liu, C. Y. Zheng, and X. T. He, Phys. Plasmas **26**, 062109 (2019).
19. F. Wang, S. Jiang, Y. Ding, S. Liu, J. Yang, S. Li, T. Huang, Z. Cao, Z. Yang, X. Hu, W. Miao, J. Zhang, Z. Wang, G. Yang, R. Yi, Q. Tang, L. Kuang, Z. Li, D. Yang, Y. Li, X. Peng, K. Ren, and B. Zhang, Matter Radiat. Extremes **5**, 035201 (2020).
20. C. Chen, T. Gong, Z. Li, L. Hao, Y. Liu, X. Liu, H. Zhao, Y. Liu, K. Pan, Q. Li, S. Li, Z. Li, S. Jin, F. Wang, and D. Yang, Matter Radiat. Extremes **9**, 027601 (2024).
21. J. D. Moody, P. Michel, L. Divol, R. L. Berger, E. Bond, D. K. Bradley, D. A. Callahan, E. L. Dewald, S. Dixit, M. J. Edwards, S. Glenn, A. Hamza, C. Haynam, D. E. Hinkel, N. Izumi, O. Jones, J. D. Kilkenny, R. K. Kirkwood, J. L. Kline, W. L. Kruer, G. A. Kyrala, O. L. Landen, S. LePape, J. D. Lindl, B. J. MacGowan, N. B. Meezan, A. Nikroo, M. D. Rosen, M. B. Schneider, D. J. Strozzi, L. J. Suter, C. A. Thomas, R. P. J. Town, K. Widmann, E. A. Williams, L. J. Atherton, S. H. Glenzer, and E. I. Moses, Nat. Phys. **8**, 344 (2012).

https://doi.org/10.1017/hpl.2025.10037 Published online by Cambridge University Press